CLEAR IMAGE CAPTURE
Active Cameras System for Tracking a High-speed Moving Object

Hiroshi Oike, Haiyuan Wu, Chunsheng Hua and Toshikazu Wada

Department of Computer and Communication Sciences, Wakayama University, 930 Sakaedani, Wakayama City 640-8510, Japan

{oike, wuhy, hua,twada}@vrl.sys.wakayama-u.ac.jp

Abstract: In this paper, we propose a high-performance object tracking system for obtaining high-quality images of a high-speed moving object at video rate by controlling a pair of active cameras that consists of two cameras with zoom lens mounted on two pan-tilt units. In this paper, "high-quality image" implies that the object image is in focus and not blurred, the size of the object in the image remains unchanged, and the object is located at the image center. To achieve our goal, we use the K-means tracker algorithm for tracking objects in an image sequence captured by the active cameras. We use the results of the K-means tracker to control the angular position and speed of each pan-tilt-zoom unit by employing the PID control scheme. By using two cameras, the binocular stereo vision algorithm can be used to obtain the 3D position and velocity of the object. These results are used in order to adjust the focus and zoom. Moreover, our system allows the two cameras to gaze at a single point in 3D space. However, this system may become unstable when the time response deteriorates by excessively interfering in a mutual control loop or by strict restriction of the camera action. In order to solve these problems, we introduce the concept of reliability into the K-means tracker, and propose a method for controlling the active cameras by using relative reliability. We have developed a prototype system and confirmed through extensive experiments that we can obtain focused and motion-blur-free images of a high-speed moving object at video rate.

1 INTRODUCTION

It is likely that a captured image may include a blurred object if the object is moving at a high speed and the camera is relatively stable. In such cases, we will lose important information (e.g., the object's edge and colors), which is required in several computer vision researches. With regard to the problems in recognizing and understanding high-speed moving objects, capturing a high-quality image is as important as analyzing the captured object image.

To solve these problems, we propose a high-performance object tracking system for obtaining high-quality images of a high-speed moving object at video rate.

1.1 Related Work

Related works on active vision tracking systems have been developed by many researchers. The following are examples of some representative researches.

(a) Active tracking system using vision chip (Komuro et al., 2003).

(b) Active tracking system using high-speed cameras (Okada et al., 2004).

(c) Object detection and tracking system using fixed viewpoint pan-tilt-zoom camera (Matsuyama et al., 2000).

(d) Active tracking system using binocular stereo heads (Bjorkman and Eklundh, 2002).

(e) Binocular pursuit system (Coombs and Brown, 1993).

(f) Visual closed-loop system using Dynamic effect (Corke and Good, 1996).

The system in (a) may be the fastest driven tracking system in the world. Since it uses a special sensor (Vision Chip), the resolution of the obtained image is quite low. Further, the system can only pursue an object in an illumination-controlled indoor room.

The system in (b) was constructed using a high-speed camera, and can thus only obtain very dark images due to the short exposure time.

The system in (c) uses an *fixed viewpoint pan-tilt-zoom camera* (hereafter referred to as an FV-PTZ

camera) similar to our system. Due to the use of background subtraction as the object tracking algorithm, the active camera must stop its motion for image capture. Therefore, moving target images captured by this system may appear blurred or out of focus. Moreover, the tracking performance of this system is a few dozen degrees per second.

System (d) was constructed using binocular cameras similar to our system. The advantage of this system is that it seldom fails in tracking a target that is at a different depth when compared to its surrounding objects. This is a fast-driven system; however, it is very expensive because it uses very complex special hardware.

In (e), the system was constructed using binocular camera head fixed on the robot arm, and In (f), it presented the effect of the introduction the dynamic control (like feed-forward control) into closed-loop tracking system. In these manuscripts, the methods of object tracking are not described clearly.

As is evident from the details stated above, the related works require complex, expensive, and special hardware; in addition, their operation is seldom stable in a real environment. Moreover, their systems obtain target object images regardless of their quality, because the architecture of these systems is based on the concept of only tracking the object.

1.2 Our Approach

In our system, we use two computers and video cameras that are available in the market to obtain the object image, track the target object, and control the active cameras at 30 fps. In our system, the camera is controlled such that it moves at the same angular speed and direction as the target object. Therefore, we can obtain an image with a blurred background and clear target at the image center (Fig.1). Additionally, we use binocular active cameras to track the object. We can then estimate the 3D position and velocity of the object. The 3D information can be used for adjusting the focus and zoom of the camera. Therefore, we can obtain target images that are clearer than those
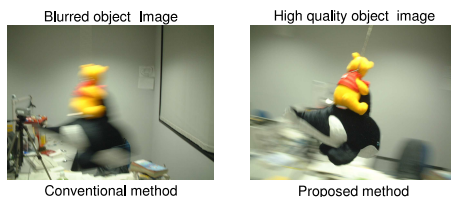

Figure 1: Obtained by conventional method (left) and proposed method (right).

obtained by using only a single active camera. The requirements for our system are as follows:

(1) binocular active cameras to focus their optic axis on a point in 3D space

(2) target to appear at the center of the images

This is because condition (1) helps us to avoid the contradiction between detection with two cameras. Epipolar geometry can work stably only if there is no contradiction between the two cameras.

Condition (2) is required because the view angle will become narrow when zooming in and the target will easily escape from the image. In such cases, the object tracking may completely fail, and thus, there will be no means to control the cameras.

In fact, it is difficult to estimate the *absolute correct epipolar line* because of the errors in object tracking or estimation of camera directions. The system becomes unstable if it is controlled according to an incorrect epipolar line. Further, the system may become unstable and lose its smoothness if the time response deteriorates under the influence of excessive interactions between the two control loops, or if the actions of the cameras are overly restricted. If the tracking system's action is not smooth, the target in the image will appear blurred and the accuracy of the object tracking will deteriorate. Therefore, the control of the active cameras will become increasingly unstable. As previously described, to focus the optic axis of two cameras on one 3D point, we must solve the following problems.

(A) The information sent from the other camera may be incorrect or of low accuracy if a tracking failure occurs.

(B) Excessive constraint from the other camera will make the tracking system's action unstable.

The conventional related studies on active vision tracking systems do not mention the methods for controlling the binocular active camera with an emphasis on the quality of the captured images by solving problems (A) and (B).

Therefore, in this paper, we have proposed a new method for solving these problems and constructing a high-speed-tracking active camera system, that can continuously obtain high quality images. Our system can automatically control the direction, zoom, and focus of the two cameras to focus on a point in 3D space.

To solve problem (A), we introduce the concept of reliability into the K-means tracker and propose a method to constrain the camera action by using this reliability, which is based on the calculation of the distance from the K-means clusters.
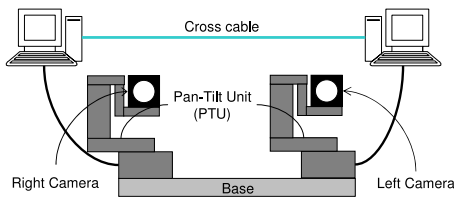
Figure 2: Construction of high-speed-tracking active cameras.

Figure 3: FV-PTZ camera(Active camera).

To solve problem (B), we propose a method for determining the level of constraint with a relative reliability.

By using our proposed methods, the binocular active cameras can be smoothly controlled and their optic axes can intersect at a point in 3D space.

2 CONSTRUCTION OF THE PROPOSED SYSTEM

We construct our high-speed-tracking active cameras with two active cameras and two computers (Fig.2). The two computers can communicate with each other and share their observations.

For the active camera in our proposed system, we employ a FV-PTZ camera (Fig.3). This camera is calibrated such that its optical center corresponds with the point of intersection of the pan and tilt axes. Therefore, the optical center of the FV-PTZ camera does not move if the pan or tilt angle is changed (Fig.4).

Therefore, by using this camera, we can ignore the movement of the optical center. As a result, it is easy
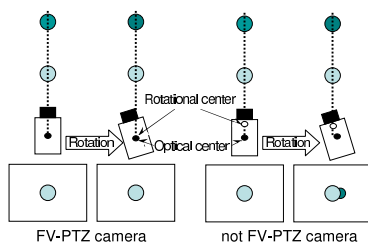

Figure 4: Particularity of FV-PTZ camera.

to estimate the angular velocity of the target from the captured image and represent the target velocity by the angular velocity of the optical center.

In our system, since two cameras are fixed on the base, as shown in Fig.2, the distance between the cameras is constant. Therefore, we can only consider the rotational relationship between the two cameras and ignore the translation of the optical center.

3 ANALYSIS OF THE OBJECT TRACKING ALGORITHM ON THE IMAGE

Numerous powerful algorithms for object tracking have been developed, such as Condensation(Isard and Blake, 1998), mean-shift(Comaniciu et al., 2003) and K-means tracker(C. Hua and Wada, 2006a; C. Hua and Wada, 2006b).

Condensation is a very robust algorithm that allows for ambiguity in the target position in the image. However, it cannot accurately estimate the target position because of this ambiguity.

For controlling the direction of the active cameras to track a moving object, the tracking algorithm must output a unique result but not an ambiguous one. Thus, we consider the mean-shift and K-means tracker algorithms to be suitable for our system.

Authors of mean-shift algorithm claim that it can adapt to variations in the target shape, color distribution, and size. However, through our experiments, we found that tracking becomes unstable if the target size varies greatly. Another problem is that when the target is monochromatic and in the plan shape, the mean-shift algorithm becomes sensitive to the color shift.

We have developed a K-means tracker algorithm that utilizes K-means clustering by using both the positive samples of the target and the negative samples surrounding the target. In this algorithm, the target feature is composed of the position as well as its color because the clustering is performed in a 5D space spanned by 3D color and 2D position parameters. This implies that this algorithm can adapt to not only target position but also the color shift of the target. Therefore, it can adapt to the shift in the illumination environment caused by changing the camera direction.

Another feature of the K-means tracker is that it can adapt to variations in the target shape and size in the image since it uses a variable ellipse model.

Thus, K-means Tracker is the most suitable algorithm for the active vision tracking system.

3.1 Summary of K-means Tracker

In the K-means tracker, robust object tracking is realized by using a variable ellipse model that is updated in each frame according to the clustering results. The pixels on the variable ellipse contour are defined as the representative non-target samples, and the area within the ellipse is the target search area.

In the first frame, we manually select some target cluster centers whose number is roughly the same as the number of colors contained by the target. In addition, we select one non-target cluster center $\mathbf{b}$ on the background for the tracking system. Then, the selected non-target center and the centroid $\mathbf{c}$ of the target centers will constitute the initial variable ellipse model in the form of a circle. The distance $\|\mathbf{c} - \mathbf{b}\|$ is the radius of this circle.

3.1.1 Clustering in the 5d Feature Space

To represent the properties of the target features in the K-means Tracker, each pixel in an image is described by a 5D feature vector $\mathbf{f} = [\mathbf{k}\ \mathbf{p}]^T$, where, $\mathbf{k} = [Y\ U\ V]^T$ describes the color similarity and $\mathbf{p} = [x\ y]^T$ describes the position approximation of the pixel. The feature vector of the i th target cluster center is represented as follows:

$$\mathbf{f}_{\mathrm{T}}(i) = [\mathbf{k}_{\mathrm{T}}(i)\ \mathbf{p}_{\mathrm{T}}(i)]^{\mathrm{T}} \quad (i = 1 \sim \mathrm{n}). \tag{1}$$

The feature tor of the j th non-target cluster center on the ellipse contour is represented as follows:

$$\mathbf{f}_{\mathrm{N}}(j) = [\mathbf{k}_{\mathrm{N}}(j)\ \mathbf{p}_{\mathrm{N}}(j)]^{\mathrm{T}} \quad (j = 1 \sim \mathrm{m}). \tag{2}$$

Here, n and m describe the number of cluster center of target and non-target, respectively.

To distinguish whether pixel u belongs to the target center or not, we calculate the distances from $\mathbf{f}_u$ to the target and non-target cluster centers, respectively.

$$d_T(\mathbf{f}_u) = \min_{i=1\sim\mathrm{n}} \{\|\mathbf{f}_{\mathrm{T}}(i) - \mathbf{f}_u\|^2\} \tag{3}$$

$$d_N(\mathbf{f}_u) = \min_{j=1\sim\mathrm{m}} \{\|\mathbf{f}_{\mathrm{N}}(j) - \mathbf{f}_u\|^2\} \tag{4}$$

Here, within the search area, $\mathbf{f}_u$ describes the feature vector at pixel u, $d_T(u)$ and $d_N(u)$ describe the distances from $\mathbf{f}_u$ to its nearest target cluster center and nearest non-target cluster center, respectively.

If $d_T(\mathbf{f}_u) < d_N(\mathbf{f}_u)$, the pixel is detected as a target pixel; otherwise, it is a non-target pixel.

3.1.2 Updating Variable Ellipse Model

To estimate the search area represented as a variable ellipse, we represent the equation of ellipse parameters as a relation of the Mahalanobis distance and the Gaussian probability density function.

$$[\mathbf{y} - \mathbf{c}]^{\mathrm{T}} \overline{\Sigma}^{-1} [\mathbf{y} - \mathbf{c}] = J \tag{5}$$

Where,

$$J = -2\ln(1 - \frac{P}{100}) \tag{6}$$

$$\overline{\Sigma} = \frac{1}{e} \sum_{\mathbf{y} \in S} [\mathbf{y} - \mathbf{c}][\mathbf{y} - \mathbf{c}]^{\mathrm{T}}. \tag{7}$$

Equations (5), (6), and (7) indicate that the search area ellipse will contain P % of the target pixels existing within the ellipse when applying Gaussian probability function is applied to fit to the set of target points (Fig. 5).). This has the added effect of removing outlying pixels.
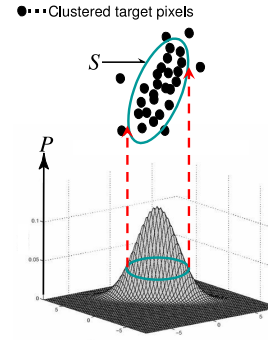

Figure 5: Estimation of the ellipse parameter by using Mahalanobis distance and Gaussian probability density function.

The center $\mathbf{c}$ of the variable ellipse at the next frame is calculated as follows:

$$\mathbf{c} = \frac{1}{e} \sum_{\mathbf{y} \in S} \mathbf{y}. \tag{8}$$

Here, S describes the pixel set inside the ellipse; e describes the number of target pixels inside the ellipse; and $\mathbf{y} = [y_x, y_y]^{\mathrm{T}}$ describes the target pixels.

In our system, we use $\mathbf{c}$ to represent the target center. By updating $\mathbf{c}$ in every frame, our system can track the target and estimate its angular velocity.

4 PROCESS FLOW

The K-means tracker discriminates each pixel within the search area into a target and non-target pixel. In our method, based on this discrimination, we propose the concept of reliability into the K-means tracker. The reliability represents how similarly each pixel belongs to each target cluster. With this reliability, our proposed system can determine which camera tracks the target more correctly and restrain the action of the camera with a lower reliability based on the output of the higher one.
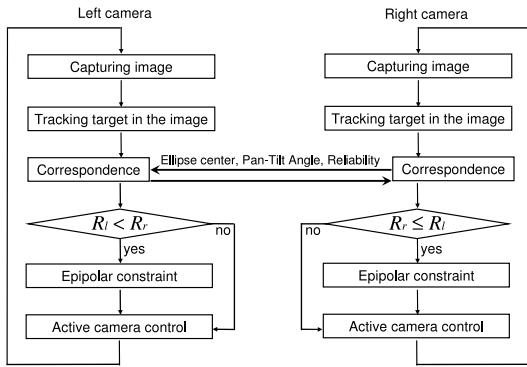
Figure 6: Flow chart of the our system.

In Fig.6, we show the flowchart of our proposed active camera system where the constraint on the camera action is based on the reliability. The reliability of the left and right cameras is described by R_l and R_r, respectively. The left and right active cameras can be independently controlled using the result of K-means tracker. In such cases, each camera can independently track the target, but it cannot automatically control the zoom and focus.

Our system tracks the target in the images captured from both cameras by using the K-means tracker. It then estimates the target position in the each image. With this position information, the direction from each optical center to the target can be calculated.

With the result of K-means tracker, we can calculate the reliability of each camera. We can then estimate the epipolar line on the lower reliability camera according to the target position in the image captured by the higher reliability camera. The ellipse center in the image taken from the lower reliability camera is constrained on the estimated epipolar line. Since the optical axis of the active camera is controlled based on the target position in the image, the optical axis of the active camera with the lower reliability is constrained on the estimated epipolar line. If the optical axis constrains the ellipse position excessively, the FV-PTZ unit response is lost; the velocity and direction of the active cameras will then be different from those of the tracked target. Due to these reasons, the tracking system may easily become unstable.

To solve this problem, we propose a method in which the ellipse position is not completely constrained on the epipolar line but is weighted by the higher reliability value of the higher reliability camera.
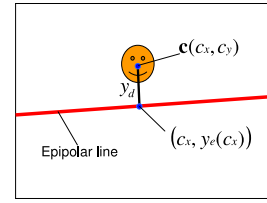

Figure 7: Ellipse position constraint on the epipolar line along the vertical direction.

4.1 Calculation of the Reliability

The reliability of each camera is calculated according to the result of the distance calculated in the feature space of the K-means tracker.

In this paper, u represents a pixel in the search area restricted in an ellipse. $r(u)$ represents the reliability of u and describes the similarity of target clusters. $r(u)$ is calculated as follows:

$$r(u) = \begin{cases} \frac{d_N(\mathbf{f}_u)}{d_N(\mathbf{f}_u) + d_T(\mathbf{f}_u)} & (d_T(\mathbf{f}_u) < d_N(\mathbf{f}_u)) \\ 0 & (otherwise). \end{cases} \quad (9)$$

Here, the distances of $d_T(\mathbf{f}_u)$ and $d_N(\mathbf{f}_u)$ are calculated by Eq.(3) and Eq.(4), respectively.

Further, R is the reliability of all pixels in the search area restricted in the same ellipse, and is calculated by

$$R = \frac{1}{e} \sum_{u=1}^{C} r(u). \quad (10)$$

Here, C is the number of pixels in the ellipse and e is the number of target pixels. To correct the difference between ellipse size of the two cameras, R is normalized by e.

4.2 Constraint Ellipse on Epipolar Line by using Relative Reliability

In our proposed system, based on the results of tracking with the high-reliability camera, the ellipse position is constrained on the epipolar line only in the low-reliability camera.

In many cases, the two epipolar lines drawn in each image become horizontal because the active cameras are fixed on the horizontal base. Therefore, the ellipse position is constrained on the epipolar line only along the vertical direction.

In Fig.7, y_d is the distance along the vertical direction from the ellipse center $\mathbf{c} = (c_x, c_y)$ to the epipolar line. $y_e(x)$ is the vertical coordinate of the intersection point of the epipolar line and the vertical line that passes through the ellipse center $\mathbf{c}$. y_d is

calculated as follows:

$$y_d = y_e(c_x) - c_y. \tag{11}$$

If the ellipse position is constrained on the epipolar line, only with y_d for a single frame, the camera action may become unstable, as described above. Thus, in our system, we let the constraint Δy be calculated by

$$\Delta y = w y_d. \tag{12}$$

Here, w is the weight of the relative reliability and is determined by

$$w = \frac{R_b}{R_l + R_r} \quad (R_b = \max\{R_l, R_r\}). \tag{13}$$

Here, R_l and R_r are calculated by Eq.(10). If the reliability of the lower reliability camera equals zero, w becomes 1, and if the reliability of the two cameras are identical, w becomes almost 0.5.

5 ACTIVE CAMERA CONTROL

In order to controlling the FV-PTZ unit, we employ the PID control scheme.

P component is assigned as the target angular velocity represented as follow:

$$\mathbf{v}_{\mathrm{obj}t} = \mathbf{v}_{\mathrm{Robj}t} + \mathbf{v}_{\mathrm{cam}t}. \tag{14}$$

Here, $\mathbf{v}_{\mathrm{Robj}t}$ and $\mathbf{v}_{\mathrm{cam}t}$ represent the relative angular velocity of the object and the rotational angular velocity of the active camera at time t. $\mathbf{v}_{\mathrm{Robj}t}$ is computed by using angle between the object center and the image center which is represented as $\mathbf{s}$.

$$\mathbf{v}_{\mathrm{Robj}t} = \frac{\mathbf{s}_t - \mathbf{s}_{(t-1)}}{\Delta t} \tag{15}$$

Here, Δt represents the time between continuous two frames. The system can know $\mathbf{v}_{\mathrm{cam}t}$ by response from PTU controller.

I component rectifies the difference between the object center and the image center and it calculated by follow:

$$\mathbf{v}_{\mathrm{dx}t} = \frac{\mathbf{s}_t}{\Delta t}. \tag{16}$$

Because the command format for PTU is angular velocity, I component has to be transformed to angular velocity form.

D component is represented by the angular acceleration calculated as follow:

$$\mathbf{a}_t = \frac{\mathbf{v}_{\mathrm{obj}t} - \mathbf{v}_{\mathrm{obj}(t-1)}}{\Delta t}. \tag{17}$$

Thus, the PID control scheme is suitable for simultaneously controlling the angular speed and position of the pan-tilt unit. Therefore, the PID-based
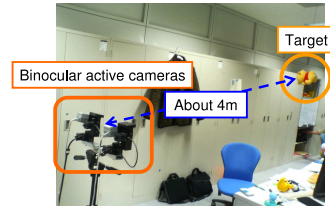

Figure 8: The Environment of Comparative Experiments.

pan-tilt control is effective for motion synchronization between the target and the active camera.

The control value $\mathbf{v}_u$ is computed by

$$\mathbf{v}_{\mathrm{u}t} = \mathrm{K}_{\mathrm{p}}\mathbf{v}_{\mathrm{obj}t} + \mathrm{K}_{\mathrm{i}}\mathbf{v}_{\mathrm{dx}t} + \mathrm{K}_{\mathrm{d}}\mathbf{a}_t\Delta t. \tag{18}$$

Furthermore, using the proposed system, we can obtain 3D position information of the target because two cameras are used. Therefore, the system can automatically control each camera's zoom and focus based on the estimated distance from the cameras. In our system, zoom is controlled for keeping the resolution of the target appearance.

Focus is controlled based on the relationship between the distance and the best focus value which has already been known by pre-experiment.

6 EXPERIMENT

6.1 Comparative Experiment

We carried out comparative experiments to verify the performance of our proposed tracking system by comparing it with two other methods.

Method 1: Epipolar constraint is not used to control the active cameras. This implies that the two active cameras are controlled independently.

Method 2: The epipolar constraint is applied to the camera with the lower reliability and the weight factor is set as $w = 1$.

Method 3: The proposed method. The epipolar constraint is applied to the camera with the lower reliability and the weighted quantity of the constraint with a relative reliability is used.

Figure 8 shows the environment in which the comparative experiments were performed.

The target object is a doll suspended from the ceiling and swinging like a pendulum. In this experiment, the doll was at a distance of about 4 meters from the active cameras in the initial state.

We show a part of the sequence obtained in this experiment as captured by the right camera in Fig.9.

Method.1   Method.2   Method.3

Figure 9: Several frames of the sequence obtained in the experiment.

To compare the three methods impartially, we allow the tracked target to assume the same motion in each experiment. We release the target object at the same height and allow it to move with an inertial motion three times.

The red lines in Fig.9 indicate the visual line of the left camera projected onto the image of the right camera.

To evaluate the performance of: *Controlling the binocular active camera to make the direction of the cameras intersect at a point in 3D space*, we used the error of the visual lines of the cameras and compared this among the three methods. As an evaluation measure, the error between each normalized vector of the epipolar planes calculated based on each camera was used. If the visual lines of the cameras perfectly intersect at a point, the error between each normalized vector will be zero.

We tracked the target object during 120 frames and calculated the absolute average and deviation of the errors between each normalized vector. Fig.10 shows a graph that indicates the error between each normalized vector with time and the absolute average and deviation of the error is shown in Table 1.

The error between each normalized vector in Method 3 was less that in Method 1. Therefore, our proposed method effectively achieves our goal. The error between each normalized vector in Method 2 was greater than that in the other two methods.

This is because the control of the directions of the active cameras became unstable since they could not respond quickly when the estimated ellipse center was constrained on the epipolar line. Next, we demon-

Table 1: Average and deviation of the error between each normalized vector(unit: degree).

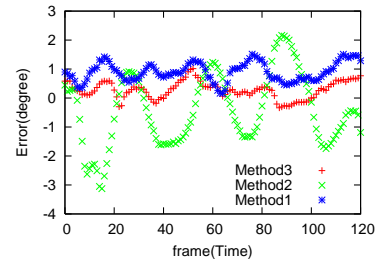| Method	Ave	Dev
1	0.84	0.28
2	1.06	0.71
3	0.33	0.20

Figure 10: The error between each normalized vector.

strate the target pursuit of our proposed system. To evaluate it, we use the difference between the rotational velocities of the target and the active camera. This is calculated as the difference between the target ellipse center axis of the image in the current frame and that in the previous frame. We call this difference *position error between frames*. This number is equal to zero if the rotational velocity of the target equals that of one of the active cameras. On the contrary, if there is a difference between the velocities, the position error between frames increases.

In Table 2, we show the average and deviation of the absolute value of the position error between frames of both the cameras when experiments were conducted using Method 1 and Method 3.

The vertical deviation in Method 3 was marginally greater than that in Method 1 while the horizontal values were almost constant.

According to the result of this experiment, we verified that the tracking performance that uses the proposed epipolar constraint method will not degrade.

6.2 Tracking a Human Head

Figure 11 show several sequential frames that track a human head. The person in these frames walked

Table 2: The average and deviation of the absolute value of the position error between frames (unit: degree).

Method:direction	Ave	Dev
1:horizontal	3.8	2.7
3:horizontal	3.7	2.5
1:vertical	3.5	2.2
3:vertical	3.8	2.9

Table 3: The average and deviation of the absolute value of the horizontal position error between frames in the human head tracking experiment (unit: degree).

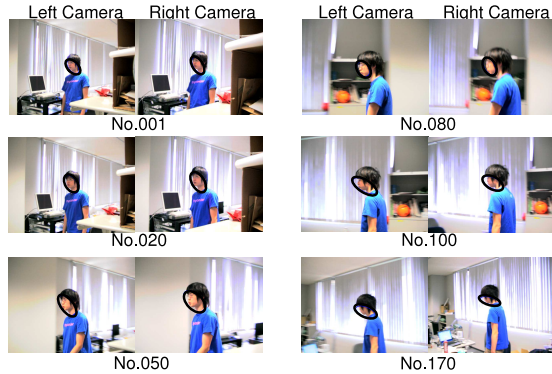| Right camera		Left camera		Summary	
Ave	Dev	Ave	Dev	Ave	Dev
2.4	2.6	2.1	2.2	2.2	2.4

Figure 11: Several frames in the sequence that track a human head.

straight from right to left. In frame no. 080, the person was closest to the cameras.

Table 3 shows the average and deviation of the absolute values of the horizontal position error between frames in the human head tracking experiment.

Because both the velocity and acceleration of the target were less than those in experiment **6.1**, the tracking error was smaller.

6.3 Zoom and Focus Control

Figure 12 shows several sequential frames that track a ball with automatic zoom-focus control. The purpose of the zoom and focus control is to maintain the tracked target in focus with constant resolution.

In order to test the effect of focus control, the target was defocused in the first frame. By comparing the images of the right camera with those of the left camera, it was observed that the size of the ball in the left camera images became smaller than that in the first frame. In contrast, the ball size in the right camera images remained unchanged because of the zoom control, which automatically zoomed in when the ball moved away from the camera.

Moreover, the defocus state in the first frame was automatically canceled by the focus control and the ball in the image was focused.
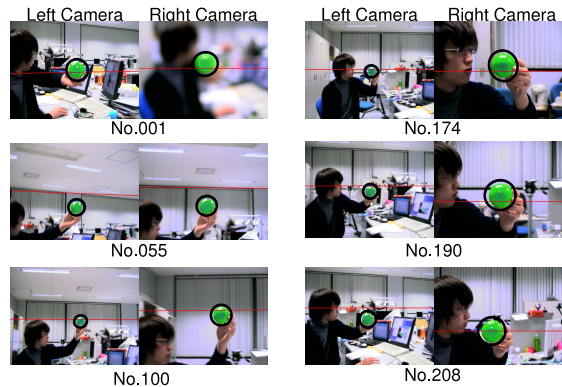

Figure 12: Several frames in the sequence for tracking a target in the zoom-focus control experiment.

7 CONCLUSION

In this paper, we have developed a high-performance object tracking system that can successfully capture high-quality images of a high-speed moving object at video rate. To increase the robustness and accuracy of object tracking in the video image, we introduced the concept of reliability into the *K-means Tracker*. In order to follow the movement of the object, two active cameras were controlled so that the object appeared at the center of the image plane. This was realized by positioning the optic axis of the two active cameras at the center of the object in the 3D space. To achieve this, we proposed the concept of relaxed epipolar constraint between the two cameras based on the reliability of object tracking and applied it to the control loop of the two active cameras. The extensive comparative experimental results demonstrated the usefulness and the effectiveness of our proposed method.

ACKNOWLEDGEMENTS

REFERENCES

Bjorkman, M. and Eklundh, J. O. (2002). Real-time epipolar geometry estimation of binocular stereo heads. *PAMI*, 24-3:425–432.

C. Hua, H. Wu, Q. C. and Wada, T. (2006a). Kmeans tracker: A general tacking algorithm for tracking people. *Journal of Multimedia*, 4.

C. Hua, H. Wu, Q. C. and Wada, T. (2006b). Object tracking with target and background samples. *IEICE (accepted)*.

Comaniciu, D., Ramesh, V., and Meer, P. (2003). Kernel-based object tracking. *PAMI*, 25-5:564–577.

Coombs, D. and Brown, C. (1993). Real-time binocular smooth pursuit. *International Journal of Computer Vision*, 11-2:147–165.

Corke, P. I. and Good, M. C. (1996). Dynamic effects in visual closed-loop systems. *IEEE transaction on Robotics Automation*, 12-5:671–683.

Isard, M. and Blake, A. (1998). Condensation-conditional density propagatiojn for visual tracking. *IJCV*, 29-1:5–28.

Komuro, T., Ishii, I., Ishikawa, M., and Yoshida, A. (2003). A digital vision chip specialized for high-speed target tracking. *IEEE transaction on Electron Devices*, 50:191–199.

Matsuyama, T., Hiura, S., Wada, T., Murase, K., and Yoshioka, A. (2000). Dynamic memory: Architecture for real time integration of visual perception, camera action, and network communication. *CVPR*, pages 728–735.

Okada, R., Oaki, J., and Kondo, N. (2004). High-speed computer vision system for robot. *TOSHIBA Review (in Japanese)*, 59-9:29–32.